Electric Properties of Chiral Plasma Plumes Without External Magnetic Field

Dan Dan Zou, Qing Zhao Ji, Yu Zhang, Oleg V. Kravchenko, Jyoti K. Atul, and Kostya (Ken) Ostrikov

***Abstract*— Helical and chiral plasma structures are ubiquitous, especially in nuclear fusion devices and space plasmas. However, the spontaneous formation of helical structures has rarely been noticed in non-equilibrium cold plasma jets that have wide applications in biomedicine and material science. Recently the chiral plasma plume without any notable asymmetry has been discovered. Under the specific parameters of pulsed discharges, the plasma bullets that at the beginning propagated in the straight lines spontaneously turn into 3-D helical discharge trajectories. Here, the electromagnetic mechanism for the chiral plasma plumes is clarified by the numerical investigation of the 3-D electromagnetic field. According to the specific standing-wave mode with the periodic poloidal component in simulation, a type of plasma plume which shows the apparent poloidal rotation only at the periodic position of the tube and moves nearly in a straight line at other positions is revealed. These findings are relevant to the development of high-voltage active electromagnetic media for artificial 3-D optical meta-material devices and precise 3-D materials processing involving helical and chiral patterns in diverse fields.**

***Index Terms*— Chiral structure, dielectric breakdown, numerical simulation, plasma plume, surface waves.**

I. Introduction

ATMOSPHERIC-PRESSURE plasma jets produce non-equilibrium cold plasmas in an open environment, instead in limited discharge gaps as conventional dielectric barrier discharges [1], [2]. It has attracted much attention for its widespread applications in plasma biomedicine, materials processing, and nanotechnology [3], [4], [5], [6], [7], [8], [9], [10], [11], [12], [13], [14], [15], [16], [17], [18]. In recent years, a new type of discharge with plasma bullets propagating in helical shapes induced by pulsed dc powers was reported in [19], [20], [21], [22], [23], [24], [25], and [26]. Without any external background magnetic field, the typical plasma plumes in helical shape form within an axisymmetric experimental set-up spontaneously, and possess two different chiral orientations (right and left hands). These patterns resemble the common helical and chiral structures in biology and materials engineering that significantly affect the properties of materials.

Furthermore, previous experimental studies by high-speed cameras revealed that the chiral plasma plumes propagate at a speed higher than 10^4 m/s and with the form of ionization waves (streamers) [21]. Recent theoretical studies found that this unusual discharge phenomenon is related to the three-dimensional helical patterns of the electric field under the specific discharge parameters [21], [22].

However, the main reason for the chirality selection is not yet clear for the helical plasma structures. Efforts in experiments have been made to add metal helical coils (with or without applied potential) on the external interface of the dielectric tubes to observe their effects on the plasma plume [23], [24]. These experiments revealed that the chiral plasma bullets in an intensified charge-coupled device (ICCD) can be guided by the outer mounted coils, and an electrostatic model has been established. While the mechanism of the formation of the helical plasma plume for the situation without the external coils is still unclear.

In this article, the configurations of the electric field without any coil are analyzed by the corresponding electromagnetic model. The studies reveal that the poloidal electric field of the standing wave is related to the origin of the helical patterns in the plasma plumes.

II. Simulation Geometry Guided by the Experimental Set-Up

The geometry and the structure of the experimental set-up representative of previous experimental works [21] without an external coil, used in the simulations here, is shown in Fig. 1. The chiral plasma plume is excited inside the dielectric tube with a length of 1 m. The inner diameter of the quartz tube is 6 mm, and the outer diameter is 9 mm. The electrode with high voltage is made of copper and covered with columnar quartz

Manuscript received 25 April 2022; revised 17 July 2022; accepted 2 September 2022. Date of publication 15 November 2022; date of current version 4 January 2023. This work was supported in part by the National Natural Science Foundation of China under Grant 12005061, in part by the State Key Laboratory of Performance Monitoring and Protecting of Rail Transit Infrastructure through the Open Project under Grant HJGZ2021109 and Grant GJJ210648, in part by the Jiangxi Province Key Research and Development Program under Grant 20202BBE53022, and in part by the Jiangxi 03 Special Project under Grant 20212ABC03A20. The review of this article was arranged by Senior Editor F. Taccogna. *(Corresponding author: Dan Dan Zou.)*

Dan Dan Zou is with the State Key Laboratory of Performance Monitoring and Protecting of Rail Transit Infrastructure, East China Jiaotong University, Nanchang, Jiangxi 330013, China (e-mail: ddzou@ecjtu.edu.cn).

Qing Zhao Ji and Yu Zhang are with the State Grid Jiangxi Electric Power Research Institute, Nanchang 330096, China.

Oleg V. Kravchenko is with the Department of Higher Mathematics, Bauman Moscow State Technical University, Moscow 105005, Russia, and also with the Federal Research Centre CSC RAS, Moscow 119333, Russia (e-mail: ok@bmstu.ru).

Jyoti K. Atul is with the Indian Institute of Geomagnetism, Navi Mumbai 410218, India.

Kostya (Ken) Ostrikov is with the School of Chemistry and Physics, Queensland University of Technology (QUT), Brisbane, QLD 4000, Australia (e-mail: kostya.ostrikov@qut.edu.au).

Color versions of one or more figures in this article are available at https://doi.org/10.1109/TPS.2022.3217859.

Digital Object Identifier 10.1109/TPS.2022.3217859

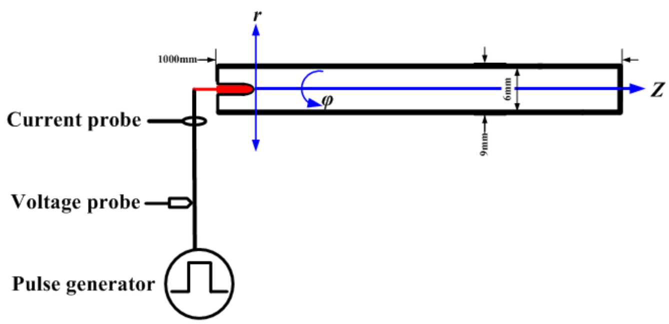

Fig. 1. Geometry and coordinates inside the tube for the electromagnetic model of chiral streamers. The dc pulse generator is shown to indicate the way to generate the plasma discharges.

dielectric. It is fixed into the left side of the tube, and with a length of 15 mm. The pulsed voltage of 6 kV is applied to the electrode, with a pulse repetition frequency of 700 Hz, and with pulsewidth fixed at 3 μs. The structure of the set-up is similar to the combination of the metal dipole antenna and the linear plasma surface wave antenna [27]. The inner part of the single needle electrode connected with the pulse power supply is made of copper and is similar to a metal dipole antenna. The outer surface of the electrode covered with columnar quartz dielectric is similar to the set-up of a linear plasma surface wave antenna. The surface electromagnetic waves resonate in the dielectric tube, exciting a poloidal standing wave mode.

III. Electromagnetic Model of Chiral Plasma

A. Symmetry Breaking: Existence of the Poloidal Electric Field

The helical trajectory of the plasma in experiments [21], [22], [23] implies the presence of the electric field with both the axial and poloidal components. However, the electrostatic model cannot explain the initial formation mechanism of the rotational electric field in poloidal orientation when applied without any coils. Therefore, the effects of the electromagnetic field excited by pulse dc discharges should be considered and the electromagnetic model should be applied instead.

To explain the formation mechanism of the poloidal electric field in chiral plasma, we consider the electromagnetic effects in the discharge. For sinusoidal excitation at an angular frequency ω, all fields have a time dependence $\exp(-j\omega t)$ and Maxwell's equations reduce to

$$\nabla \times \mathbf{E} = -j\omega\mu\mathbf{H} \quad (1)$$

$$\nabla \times \mathbf{H} = \quad j\omega\varepsilon\mathbf{E} \quad (2)$$

where $\mathbf{E}$ and $\mathbf{B}$ represent the electric and magnetic field vectors respectively. ε is dielectric constant, and μ is magnetic permittivity. The plasma is treated as a lossy dielectric with a relative permittivity [1]

$$\varepsilon_p = 1 - \frac{\omega_p^2}{\omega(\omega - j\nu_m)} \quad (3)$$

where $\omega_p = (e^2 n_e / m\varepsilon_0)^{1/2}$ is the plasma frequency, e stands for the electron, n_{e} represents the density of electrons, m is electron mass, and ν_m is the electron–neutral momentum transfer frequency. Under the cylindrical geometry coordinates (r, φ, z) setting aside the electric field component in z axis, let $\mathbf{H} = H_z\mathbf{e_z}$ and $\mathbf{E} = E_r\mathbf{e_r} + E_\phi\mathbf{e}_\phi$. Here, E_r is the radial component of the electric field, E_φ is the poloidal component of the electric field. Thus, the following relations arise:

$$\frac{1}{r}\frac{\partial}{\partial r}\left(rE_\varphi\right) - \frac{1}{r}\frac{\partial E_r}{\partial \varphi} = -j\omega\mu_0 H_z \quad (4)$$

$$-\frac{\partial H_z}{\partial r} = j\omega\varepsilon_0\varepsilon_p E_\varphi \quad (5)$$

$$\frac{1}{r}\frac{\partial H_z}{\partial \varphi} = j\omega\varepsilon_0\varepsilon_p E_r. \quad (6)$$

Then, the wave equation of the electromagnetic field after some algebra can be written as follows:

$$\frac{1}{r}\frac{\partial}{\partial r}\left(\frac{r}{\varepsilon_p}\frac{\partial H_z}{\partial r}\right) + \frac{1}{r}\frac{\partial}{\partial \varphi}\left(\frac{1}{\varepsilon_p r}\frac{\partial H_z}{\partial \varphi}\right) + k_0^2 H_z = 0 \quad (7)$$

$$E_r = \frac{-j\omega\mu_0}{k_0^2\varepsilon_p r}\frac{\partial H_z}{\partial \varphi} \quad (8)$$

$$E_\varphi = \frac{j\omega\mu_0}{k_0^2\varepsilon_p}\frac{\partial H_z}{\partial r} \quad (9)$$

where $k_0 = \omega(\varepsilon_0\mu_0)^{1/2}$ is the free space wavenumber, ε_0 is the dielectric constant of vacuum, and μ_0 is the magnetic permittivity of vacuum. H_z is axial component of the magnetic field induced by the pulse dc power supply.

To understand the nature of the wave propagation and skin effects, we consider a model [1] at the initial stage of the discharge

$$\frac{\partial^2 H_z}{\partial r^2} + \frac{1}{r}\frac{\partial H_z}{\partial r} + \frac{1}{r^2}\frac{\partial^2 H_z}{\partial \varphi^2} + \varepsilon_p k_0^2 H_z = 0. \quad (10)$$

Let

$$H_z(r, \phi, z) = R(r)G(\phi)e^{-\beta z} \quad (11)$$

where R and G are the arbitrary functions of r and φ, and substitute it into (10), one obtains

$$\frac{r^2}{R}\frac{d^2 R}{dr^2} + \frac{r}{R}\frac{dR}{dr} + \varepsilon_p k_0^2 r^2 = -\frac{1}{G}\frac{d^2 G}{d\varphi^2}. \quad (12)$$

The right side and left side of (12) should equal to a constant for any r, φ then

$$\frac{d^2 G}{d\varphi^2} = -m^2 G \quad (13)$$

$$r^2\frac{d^2 R}{dr^2} + r\frac{dR}{dr} + \left(\varepsilon_p k_0^2 r^2 - m^2\right)R = 0. \quad (14)$$

Equations (13) and (14) can be solved as

$$G = C_1 \cos m\varphi + C_2 \sin m\varphi \quad (15)$$

$$R(r) = C_3 J_m\left(k_0\sqrt{\varepsilon_p} r\right) \quad (16)$$

where $J_m(k_0(\varepsilon_p)^{1/2} r)$ is the first kind of mth order Bessel function, C_1, C_2, and C_3 are the arbitrary constants, consequently

$$H_z(r, \phi, z) = H_0 J_m\left(k_0\sqrt{\varepsilon_p} r\right) \times [C_1 \cos m\phi + C_2 \sin m\phi]e^{-\beta z}. \quad (17)$$

The poloidal electric field can be written in the following form:

$$E_\phi = \frac{j\omega\mu_0 H_0}{k_0\sqrt{\varepsilon_p}} J_m'\left(k_0\sqrt{\varepsilon_p} r\right)[C_1 \cos m\phi + C_2 \sin m\phi]e^{-\beta z}. \quad (18)$$

When $m = 0$, (18) transforms to

$$E_\phi(r,\phi,z) = E_0 J_0'\left(k_0\sqrt{\varepsilon_p} r\right)e^{-\beta z}. \quad (19)$$

From (19), for $r = 0$, the first derivative of the zeroth-order Bessel function equals 0 for any k_0 and $\varepsilon_p$values as $J_0'(k_0(\varepsilon_p)^{1/2}r) = 0$. With the increase of $r$in radial direction, $J_0'(k_0(\varepsilon_p)^{1/2}r)$ also increases. Thus, (19) demonstrates that the poloidal component of the electric field equals 0 in the axis of the tube and increases along with r variable growth.

B. Electromagnetic Mode With Periodic Structure

The electromagnetic mode proposed in (19) has a poloidal component that can explain the rotation nature of the streamers along the poloidal direction. However, the poloidal electric field component in (19) is exponentially monotonically decayed along the axial direction z of the dielectric tube. While in experiments, the plasma plumes can produce stable filaments and have a periodic structure distribution along the axial direction [21]. It is thus necessary to find a periodic poloidal electromagnetic mode to explain this experimental phenomenon.

Consider only the poloidal component of the electric field in cylindrical coordinates $\mathbf{E} = E_\varphi \mathbf{e}_\varphi$. By substituting it into Maxwell's equations (1) and (2), one obtains

$$\frac{\partial E_\varphi}{\partial z} = j\mu_0\omega H_r \quad (20)$$

$$\frac{\partial\left(rE_\varphi\right)}{r\partial r} = -j\mu_0\omega H_z \quad (21)$$

$$\frac{\partial H_r}{\partial z} - \frac{\partial H_z}{\partial r} = j\varepsilon_0\varepsilon_p\omega E_\varphi. \quad (22)$$

The wave equation in cylindrical coordinates can be obtained by combining the above equations as follows:

$$r^2\frac{\partial^2 E_\varphi}{\partial z^2} + r\frac{\partial E_\varphi}{\partial r} + r^2\frac{\partial^2 E_\varphi}{\partial r^2} + \left(\varepsilon_p k_0^2 r^2 - 1\right)E_\varphi = 0. \quad (23)$$

Substitute $E_\varphi = G(r)f(z)$ into wave equation (23), then

$$\frac{1}{G}\frac{d^2G}{dr^2} + \frac{1}{rG}\frac{dG}{dr} + \frac{\varepsilon_p k_0^2 r^2 - 1}{r^2} = -\frac{1}{f}\frac{d^2 f}{dz^2} = \eta^2. \quad (24)$$

By the method of separating variables, η is a constant which is independent of spatial coordinates, one may achieve

$$\frac{1}{G}\frac{d^2G}{dr^2} + \frac{1}{rG}\frac{dG}{dr} + \frac{\varepsilon_p k_0^2 r^2 - 1}{r^2} = \eta^2 \quad (25)$$

$$\frac{d^2 f}{dz^2} + \eta^2 f = 0. \quad (26)$$

The solution of (25) and (26) by variable separation method is as follows:

$$G(r) = A_1 J_1\left(\sqrt{\varepsilon_p k_0^2 - \eta^2} r\right) + A_2 Y_1\left(\sqrt{\varepsilon_p k_0^2 - \eta^2} r\right) \quad (27)$$

$$f(z) = B_1 \cos\eta z + B_2 \sin\eta z \quad (28)$$

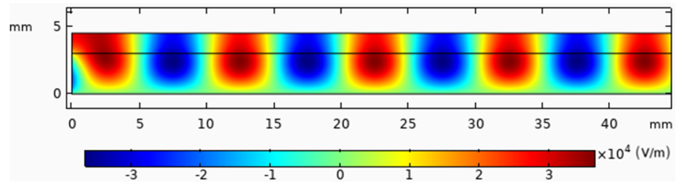

Fig. 2. Simulation results of the poloidal electric field of the standing electromagnetic wave in 2-D cylindrical coordinate system.

where A_1, A_2, B_1, and B_2 are the arbitrary constant, $J_1(\cdot)$ is the first kind of the first-order Bessel function, and $Y_1(\cdot)$ is the second kind of the first-order Bessel function. Function (28) is actually a cosine function. It can be transformed into $f(z) = (B_1^2 + B_2^2)^{1/2}\cos(\eta z + \varphi - (\pi/2))$, with $\tan\varphi = (B_1/B_2)$, and be simplified by putting $B_2 = 0$, assuming that the electric field is maximum at $z = 0$. Applying the boundary condition that the electric field is finite at $r = 0$, the poloidal electric field can be simplified as follows:

$$E_\varphi(r,z) = E_0 J_1\left(\sqrt{\varepsilon_p k_0^2 - \eta^2} r\right)\cos\eta z. \quad (29)$$

It shows that the solution of the poloidal electric field does not depend on the poloidal angle. It can be deduced that the rotation speed of the bullets in the poloidal direction is uniform along the poloidal direction, which is helpful for estimating the poloidal speed through the ICCD image in the experiment. The shear of the electric field can be written as

$$\frac{dE_\varphi}{dz} = -\eta E_0 J_1\left(\sqrt{\varepsilon_p k_0^2 - \eta^2} r\right)\sin\eta z. \quad (30)$$

Equations (29) and (30) demonstrate that the poloidal electric field in this special mode is sheared and depends on the axial position z, and is periodical following the cosine distribution along the dielectric tube.

C. Finite-Element Simulation for Poloidal Electric Field

To examine the existence of the poloidal electric field and its periodical structures for chiral plasma plumes, the finite element analysis for the electromagnetic model of (23) is utilized by using COMSOL. The boundary condition of the poloidal electric field at the axis ($r = 0$) is set as 0. The poloidal electric field E_φ in (23) is shown in Fig. 2. The periodic structure is formed under the boundary condition of the dielectric tube. For the simplicity of simulation, the lower half-plane of the central axis symmetry is not displayed. Except for the irregular stretching of the plasma channel near the incident position $z = 0$, which does exist near the electrode in the discharge experiment [21], the other positions of the poloidal electric field are in periodic structures of islands, which form periodic ring distribution from the 3-D view. The interval between the two periodic islands in Fig. 2 is about 9.3 mm, which is close to the pitch of the screw in the experiment [21]. The maximum amplitude of the electric field is located in the center of the island structure, which is the most vulnerable area to breakdown. It can be superimposed with the axial electric field to form a 3-D helical structure.

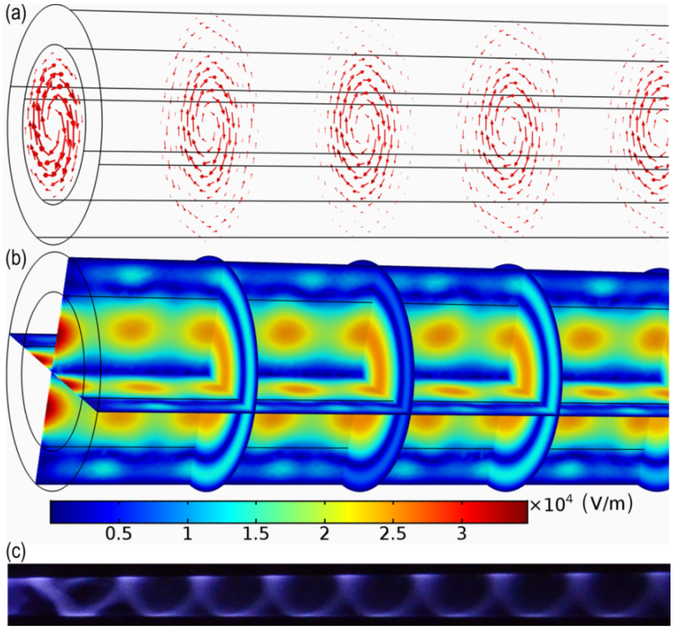

Fig. 3. (a) Simulation results of the poloidal electric field vectors and (b) electric field intensity of the standing electromagnetic wave. (c) Experimental photograph of the chiral plasma plume without external coils, applied voltage of 6 kV, pulsewidth of 3 μs, frequency of 700 Hz, and gas pressure of 4 kPa in N_2.

The simulation results of the poloidal electric field based on the electromagnetic inductive coupling model are demonstrated in Fig. 3. Equation (23) and other related equations include the dielectric permittivity of the plasma ε_p, which is related to the plasma properties in the theoretical model. While here we focus on the formation mechanism of the poloidal electric field that can guide the helical propagation of the streamer at the beginning of the discharge. And the initial state of plasma is in a quasi-neutral state, and with low electron density and temperature. The dielectric permittivity of the plasma is close to 1 under the experimental conditions. For the limit of a high-frequency, low-pressure discharge with $\nu_m \ll \omega$ as a low-loss dielectric [1], considering the initial electron density as 10^9 cm^{-3} and typical length (also wavelength) as the outer diameter of the tube, the difference in relative permittivity of the plasma is three orders of magnitude smaller than 1. Therefore, it is a good approximation to assume the relative permittivity of the plasma as 1 in the relevant equations used to analyze the origin of the poloidal electric field.

The electromagnetic wave is incident from the side of the anode in a dielectric tube, forming a TE standing wave mode with only the poloidal electric field component. Fig. 3(a) shows the slice diagram of the simulated 3-D electric field vectors. Fig. 3(a) shows that the poloidal electric field rotates around the central axis of the tube at the cross section in a rotation pattern. The electric field intensity is 0 at the center of the tube, then increases along the radial direction, with the maximum near the tube wall. If the axial electric field of the electrode is considered, a 3-D helical electric field configuration can be formed. Fig. 3(b) shows the spatial distribution of the electric field intensity in the slice diagram of the simulation, with the maximum electric field intensity being about 3.5 $\times$ 10^4 V/m, which is much less than the electric field induced by the external coil. It explains why the chiral plasma plume followed the external coil when it was added to the experiment. The result shows that the electric field intensity varies periodically along the axial direction, and forms a periodical ring inside the tube. It can be inferred that the head of streamers only has maximum rotation force on these periodic rings. Fig. 3(c) shows the specific plasma plume found in the discharge experiment [21]. It has obviously poloidal rotation only at the specific periodic position of the tube and is nearly in linear motion at other positions, which is consistent with the distribution of the electric field in the simulation. The brightness of the plasma plume in the photograph reflects the intensity of the discharge. The simulation results are placed along with the experimental photograph to compare the consistency of the periodic structures in the numerical studies and the experimental observations.

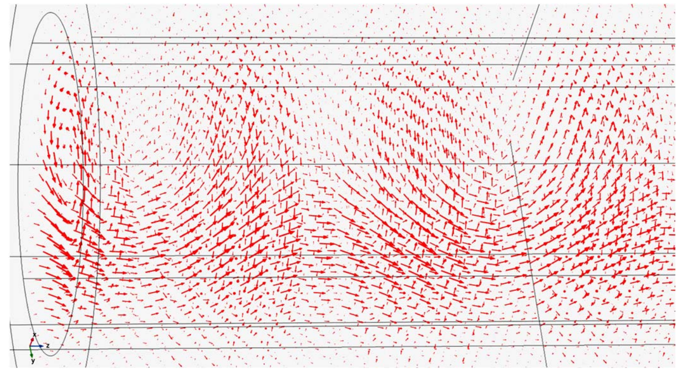

Fig. 4. Simulation results of the electric field vectors with both poloidal and axial components.

Following the single-walled carbon nanotubes (SWCNTs) analogy, the ratio of the poloidal electric field to the axial electric field in chiral plasma is like "chiral numbers" in SWCNTs. When the ratio is close to 1, the superposed poloidal electric field is close to the axial electric field in discharges, and the streamer propagates along the helical trajectory. When the ratio of the poloidal electric field to the axial electric field approaches 0, and the superimposed poloidal electric field is much smaller than the axial electric field at this position, the circular motion of the streamer along the poloidal direction can be ignored, then the discharge returns to the linear discharge mode along the axis of the tube. Moreover, the modes of different ratios may be superimposed at the same time and at different positions of the axis, so that the transition modes described in the literature appear in these mixed modes [21], [22], [28], [29], [30], [31].

When the axial electric field and the polar electric field are superposed, the electric field vector line distribution is shown in Fig. 4. It can be seen from Fig. 4 that when there is an axial electric field on one side of the tube wall, the axial electric field will be related with the polar electric field component of the ring structures, forming a helical distribution similar to Fig. 3(c).

It should be noted that there is still a gap between Fig. 4 with the normal mode of standing electromagnetic wave in a long dielectric tube under the chosen boundary condition and the breakdown electric field distribution of plasma. The electric field of streamers will change with time due to the space charge propagation in the head. And the plasma propagation of the streamer head may influence the structure of the standing electromagnetic wave after the gas breakdown. From the chiral plasma experiments without external guiding coils [21], [22], [26], the pitch of the helical plasma plume can be slightly affected by the applied voltage of the electrode that varies the plasma parameters. However, it does not change the magnitude order of the pitch and it does not break the ring structures of the plasma plumes. It is thus reasonable to assume that the effect of the plasma propagation on the structure of the standing electromagnetic wave is small. On the other hand, the standing electromagnetic wave guides the plasma plume propagation to form its helical structure. Therefore, in this work, we focus on the initial origin of the poloidal electric field that affects the chiral structure of the helical streamer. The above assumption is justified below by comparing the amplitudes of the standing electromagnetic wave and the discharge breakdown voltage. With the gas discharge parameters in experiments (gas pressure 4 kPa in nitrogen, with the gas constant $A = 12\ \text{cm}^{-1} \cdot \text{torr}^{-1}$ and $B = 342(\text{V/cm} \cdot \text{torr})$ [32], the break-down electric field magnitude is estimated to be 1.8×10^5 V/m [25]. While to form the helical structure of the plasma plume, the magnitude of an electric field in the standing electromagnetic (EM) wave is much lower than that. The analysis of chiral plasmas guided by external coils suggests that the electric field magnitude of the helical coil that can guide the discharge path to form the helical structure is of the order of 10^4 V/m [25].

The magnitude of the electric field which depends on the experimental parameters can be calculated by the radiation model of the electric dipole [33]

$$\mathbf{E}(r,t) = \mathbf{e}_r dl \frac{\eta_0}{2\pi}\frac{rz}{R^2}\left\{\frac{3i}{R^2} + \frac{1}{cR}\frac{\partial i}{\partial u}\right\} + \mathbf{e}_z dl \frac{\eta_0}{2\pi}\left\{\left[\frac{3z^2}{R^2} - 1\right]\frac{i}{R^2} + \left[\frac{z^2}{R^2} - 1\right]\frac{1}{cR}\frac{\partial i}{\partial u}\right\} \tag{31}$$

where dl is the length of the electrode, η_0 is the wave impedance, c is the light speed, i is the discharge current, and $u = t - R/c$ is the time delay of radiation propagating to the field point. In this approximation, the magnitude of the radiation field is proportional to $\partial i/\partial t$ and inversely proportional to the distance R. The value $\partial i/\partial t$ can be estimated to be the ratio of discharge current to the rise time of pulse discharge. With the rise time of the pulsed discharge of 60 ns, and the average discharge current of 0.1 mA, the magnitude of the electric field in the boundary can be estimated to be 4×10^4 V/m [21]. We emphasize that the peak value of the pulse current in the chiral discharge experiment can be higher than 10 mA and reaches about 100 mA in the experiment with grounded metal rings [23], [24]. Therefore, the above parameters of our calculations have been realized in the chiral plasma discharge experiments.

In real discharge experiments, the axial electric field is not stationary or homogeneous. The chiral plasma plume is formed by the fast plasma bullet which is a dynamic process of propagation of the ionization wave. The analysis of the plasma dynamic processes has been carried out using 2-D fluid simulations [3], [5]. However, to avoid the full coupled fluid and Maxwell equations in a 3-D asymmetric dynamical process (which would require a huge amount of computational resources [1]), we focus on the origin of the mechanism of the poloidal electric field formation leading to the chiral characteristics of the plume. This is why here we study the initial configuration of the electric field by the superposition of the axial field from the electrode and the poloidal circular structure in the standing EM-wave.

The steady-state standing waves have also helped to understand the recent experimental observations [26] that the change of the position of the electrode, which also affects the distribution and propagation of the axial field, does not affect the formation of the chiral plasma plume. Either the pitch or the total length of the chiral plasma is the same for the different positions of the electrode [26]. Therefore, our numerical results have clarified the experimental observations related to chiral streamer propagation in low-temperature plasmas, and can also be used to guide further experiments.

IV. Discussion and Conclusion

The streamer discharge in the dielectric tube normally propagates along the axial direction of the tube. The purpose of our study is to explain the formation mechanism and characteristics of the helical plasma plume under the special discharge parameters of pulse excitation. Therefore, this article focuses on the electric field, which can initially guide the streamer to rotate in the poloidal direction and determine the orientation of chirality, as the object of our numerical calculation. Through the calculation of the electromagnetic model equations, the electromagnetic modes with the poloidal electric field have been found, and the mode can also form the axially periodic ring structure of the poloidal electric field. The length of one period of the ring structure in our numerical result is in the same order of magnitude as the length of the helical streamer pitch in the previous chiral plasma discharge experiments. Furthermore, inspired by this numerical analysis, we found in the photograph of the discharge experiment that there is indeed a phenomenon in which the helical streamer rotates at a specific periodic position and propagates in a nearly straight line at other dielectric tube positions. This important experimental phenomenon has not been noticed or mentioned in the previous literature on chiral plasma experiments. And it also confirms that the numerical results in this article can explain the experimental phenomenon formed by the electromagnetic effects on the helical streamers.

In summary, we present the first plasma model to explain the formation of chiral plasma plumes without guiding by the external coils. Our previous work [22] only contained preliminary analysis without any plasma parameters. The electromagnetic field simulation is also established for the first time to verify the existence and distribution of the poloidal electric field. The reason for the appearance of chiral plasma streamers which was hypothesized in previous works, namely, the generation of the poloidal electric field, has been validated in this article. The electromagnetic model proposes that the origin of the initial electric field in the poloidal direction comes from the electromagnetic field excited by the pulse discharges in the chiral plasma experiment without an external coil. In the simulation, electromagnetic waves incident on the electrode side forms a standing wave mode with the poloidal electric field in the dielectric tube. The poloidal electric field rotates around the axis of the tube, and the amplitude of the electric field presents a distribution in periodic rings along the axis of the tube. The helical electric field distribution forms after the superposition between the poloidal electric field and the axial electrostatic electric field generated by the electrode. Corresponding to the specific wave mode with only the poloidal component, the plasma plume which has obvious poloidal rotation only at the periodic position of the tube and moves nearly in a straight line at other positions, is found.

It is an open question why the chiral plasma plume only appears under a certain frequency. When the pulse repetition frequency is very low, the time interval between the two pulses is very long, and more residual electrons of the previous pulse diffuse and run away. It is hard to provide enough seed electrons for the next pulse to form a sustainable discharge breakdown. When frequency increases to a certain threshold, the time interval between the two pulses becomes shorter, the residual electrons from the previous pulse increase, and the difficulty of discharge decreases gradually. Under electromagnetic assistance, a helical discharge is formed first at the edge of the dielectric tube with more charges. Then, if the frequency continues to increase, after enough residual electrons are accumulated in the center of the dielectric tube, the discharge enters into the transition mode where the central straight line and the helical plume coexist. And it finally enters into the discharge mode of a central straight line completely after exceeding a certain frequency threshold.

Moreover, it is also interesting to investigate the relationship between chiral orientation and other discharge parameters. However, the chiral orientation of the plasma is not simply dependent on the pulse frequency or the pulsewidth. It is very sensitive to the complex initial and boundary condition of the discharge, such as the initial phase of the electromagnetic wave. Different rotation directions could be acquired by considering the phase position of the poloidal electric field in our simulation model. For the assumption that our model is in the frequency domain with Fourier transform, all fields in fact have a dependence $\exp(-j\omega t)$ in the time domain. The solution of the poloidal electric field (23) in the time domain also should add the term of $\exp(-j\omega t)$. The real part of the solution is in the form of $\cos(\omega t)$. In the first half of the period, the time term of $\cos(\omega t)$ is positive. While in the last half of the period, it turns negative. Multiplying the term of $\exp(-j\omega t)$ to the result of the poloidal electric field will change the poloidal rotation directions of the electric field. Then, the initial time phase of the poloidal electric field when the plasma bullet enters the tube may determine the direction of its rotation.

Last but not least, it is worthwhile to address the prospect of the proposed model. The 3-D electromagnetic simulation coupled with the reactive particles at the same time is difficult to simulate and predict. With tremendous degrees of freedom in 3-D grids, the numerical error of the simulation combined 3-D field and reactive particles will be too large to find out the physical essence. This plasma model decoupled the 3-D electromagnetic field and particles by considering the plasma as material to give the influence of particles on the field at first. And then in the future, the simulation of 3-D reactive particles' time revolution can be performed based on the field. It is a good approximation [1], [34], [35] for understanding the new physical characteristic of the helical streamer with poloidal rotation. Certainly, further experimental and numerical studies are needed for a better understanding of the specific discharge mechanism.

Acknowledgment

The authors would like to thank insightful discussions with Prof. J. Zhu.

References

[1] M. A. Lieberman, J. P. Booth, P. Chabert, J. M. Rax, and M. M. Turner, "Standing wave and skin effects in large-area, high-frequency capacitive discharges," *Plasma Sources Sci. Technol.*, vol. 11, no. 3, pp. 283–293, Aug. 2002.

[2] Y.-R. Zhang, Y.-T. Hu, and Y.-N. Wang, "How to address the issue of uniformity in large area capacitively coupled plasmas? A modeling investigation," *Plasma Sources Sci. Technol.*, vol. 29, no. 8, Aug. 2020, Art. no. 084003.

[3] X. Lu, G. V. Naidis, M. Laroussi, and K. Ostrikov, "Guided ionization waves: Theory and experiments," *Phys. Rep.*, vol. 540, no. 3, pp. 123–166, Jul. 2014.

[4] H. P. Li et al., "Translational plasma stomatology: Applications of cold atmospheric plasmas in dentistry and their extension," *High Voltage*, vol. 2, no. 3, pp. 188–199, 2017.

[5] N. Y. Babaeva and M. J. Kushner, "Interaction of multiple atmospheric-pressure micro-plasma jets in small arrays: He/O_2 into humid air," *Plasma Sources Sci. Technol.*, vol. 23, no. 1, Jan. 2014, Art. no. 015007.

[6] Y. Xian, X. Lu, S. Wu, P. K. Chu, and Y. Pan, "Are all atmospheric pressure cold plasma jets electrically driven?" *Appl. Phys. Lett.*, vol. 100, no. 12, Mar. 2012, Art. no. 123702.

[7] K. Ostrikov, E. C. Neyts, and M. Meyyappan, "Plasma nanoscience: From nano-solids in plasmas to nano-plasmas in solids," *Adv. Phys.*, vol. 62, no. 2, pp. 113–224, 2013.

[8] Y. B. Xian, D. D. Zou, X. P. Lu, Y. Pan, and K. Ostrikov, "Feather-like He plasma plumes in surrounding N_2 gas," *Appl. Phys. Lett.*, vol. 103, no. 9, Aug. 2013, Art. no. 094103.

[9] L. Liu, Y. Zhang, W. Tian, Y. Meng, and J. Ouyang, "Electrical characteristics and formation mechanism of atmospheric pressure plasma jet," *Appl. Phys. Lett.*, vol. 104, no. 24, Jun. 2014, Art. no. 244108.

[10] Y. Yue et al., "Radial constraints and the polarity mechanism of plasma plume," *Phys. Plasmas*, vol. 25, no. 10, 2018, Art. no. 103510.

[11] H. Cheng, X. Liu, X. Lu, and D. Liu, "Numerical study on propagation mechanism and bio-medicine applications of plasma jet," *High Voltage*, vol. 1, no. 2, pp. 62–73, 2016.

[12] X. Lin et al., "Chiral plasmons with twisted atomic bilayers," *Phys. Rev. Lett.*, vol. 125, no. 7, 2020, Art. no. 077401.

[13] A. Yachmenev, J. Onvlee, E. Zak, A. Owens, and J. Kupper, "Field-induced diastereomers for chiral separation," *Phys. Rev. Lett.*, vol. 123, no. 24, Dec. 2019, Art. no. 243202.

[14] A. V. Eletskii and G. S. Bocharov, "Emission properties of carbon nanotubes and cathodes on their basis," *Plasma Sources Sci. Technol.*, vol. 18, no. 3, Aug. 2009, Art. no. 034013.

[15] S. Cho, "Theory of mode conversion in helicon plasmas," *Plasma Sources Sci. Technol.*, vol. 29, no. 9, Sep. 2020, Art. no. 095023.

[16] S. Wu, Z. Wang, Q. Huang, X. Tan, X. Lu, and K. Ostrikov, "Atmospheric-pressure plasma jets: Effect of gas flow, active species, and snake-like bullet propagation," *Phys. Plasmas*, vol. 20, no. 2, Feb. 2013, Art. no. 023503.

[17] S. AkishevYu et al., "Development of a spark sustained by charging the stray capacitance of the external circuit in atmospheric-pressure nitrogen," *Plasma Phys. Rep.*, vol. 33, no. 7, pp. 584–601, 2007.

[18] C. Li, A. Ji, and Z. Cao, "Stressed Fibonacci spiral patterns of definite chirality," *Appl. Phys. Lett.*, vol. 90, no. 16, Apr. 2007, Art. no. 164102.

[19] T. Darny, E. Robert, S. Dozias, and J.-M. Pouvesle, "Helical plasma propagation of microsecond plasma gun discharges," *IEEE Trans. Plasma Sci.*, vol. 42, no. 10, pp. 2506–2507, Oct. 2014.

[20] G. Xia et al., "Atmospheric plasma jet relay driven by a 40-kHz power supply and its representative characteristics," *IEEE Trans. Plasma Sci.*, vol. 43, no. 5, pp. 1825–1831, May 2015.

[21] D. Zou, X. Cao, X. Lu, and K. Ostrikov, "Chiral streamers," *Phys. Plasmas*, vol. 22, no. 10, Oct. 2015, Art. no. 103517.

[22] D. Zou et al., "Plasma characteristics of helical streamers induced by pulsed discharges," *Acta Phys. Sinica*, vol. 66, no. 15, 2017, Art. no. 1552021.

[23] L. Nie, F. Liu, X. Zhou, X. Lu, and Y. Xian, "Characteristics of chiral plasma plumes generated in the absence of external magnetic field," *Phys. Plasmas*, vol. 25, no. 5, May 2018, Art. no. 053507.

[24] F. Liu, J. Li, F. Wu, L. Nie, and X. Lu, "Effect of external electric field on helix plasma plume," *J. Phys. D: Appl. Phys.*, vol. 51, no. 29, Jul. 2018, Art. no. 294003.

[25] D. Zou et al., "Finite element analysis of electrostatic field in chiral plasmas," *IEEE Access*, vol. 7, pp. 137048–137053, 2019.

[26] S. Jin, D. Zou, X. Lu, and M. Laroussi, "The effect of tube geometry on the chiral plasma," *Phys. Plasmas*, vol. 26, no. 9, Sep. 2019, Art. no. 093507.

[27] G. G. Borg et al., "Plasmas as antennas: Theory, experiment and applications," *Phys. Plasmas*, vol. 7, no. 5, pp. 2198–2202, 2000.

[28] I. O. Girka, O. I. Girka, and M. Thumm, "Azimuthal surface waves in cylindrical metal waveguides partially filled by magnetoactive plasma: Analysis of energy transfer," *Phys. Plasmas*, vol. 27, no. 6, Jun. 2020, Art. no. 062108.

[29] I. O. Girka, I. V. Pavlenko, and M. Thumm, "Rotation of electromagnetic energy initiated by azimuthal surface waves in coaxial metal waveguides entirely filled by plasma," *Phys. Plasmas*, vol. 27, no. 3, Mar. 2020, Art. no. 032104.

[30] A. Yu Akimov, V. P. Olefir, and N. A. Azarenkov, "Influence of azimuthal structure of surface waves on efficiency of their excitation by tubular electron beams," *Contr. Plasma Phys.*, vol. 46, pp. 817–825, Dec. 2006.

[31] S. Wang et al., "Microsecond pulse gas-liquid discharges in atmospheric nitrogen and oxygen: Discharge mode, stability, and plasma characteristics," *Plasma Processes Polymers*, vol. 18, no. 11, 2020, Art. no. 2000135.

[32] Y. P. Raizer, *Gas Discharge Physics*. New York, NY, USA: Springer, 1991.

[33] C. Wang, X. Chen, K. Tang, and P. Li, "Study on the discharge mechanism and EM radiation characteristics of trichel pulse discharge in air," *Plasma Sci. Technol.*, vol. 21, no. 5, May 2019, Art. no. 055402.

[34] K. Zhao et al., "Observation of nonlinear standing waves excited by plasma-series-resonance-enhanced harmonics in capacitive discharges," *Phys. Rev. Lett.*, vol. 122, no. 18, 2019, Art. no. 185002.

[35] M. A. Lieberman and A. J. Lichtenberg, *Principles of Plasma Discharges and Materials Processing*. Hoboken, NJ, USA: Wiley, 1994.